Arredondo, Francisco; Ledesma, Pablo; Castronuovo, Edgardo Daniel (2019) Optimization of the operation of a flywheel to support stability and reduce generation costs using a Multi-Contingency TSCOPF with nonlinear loads, *International Journal of Electrical Power & Energy Systems*, v. 104, pp.: 69-77.

DOI: https://doi.org/10.1016/j.ijepes.2018.06.042

Contents lists available at ScienceDirect

International Journal of Electrical Power and Energy Systems

journal homepage: www.elsevier.com

Optimization of the operation of a flywheel to support stability and reduce generation costs using a Multi-Contingency TSCOPF with nonlinear loads

Francisco Arredondo*, Pablo Ledesma, Edgardo Daniel Castronuovo

Department of Electrical Engineering, University Carlos III of Madrid, Avda. de la Universidad 30, 28911 Leganés (Madrid), Spain

ARTICLE INFO

Keywords:
Energy storage
Insular grid
Nonlinear programming
Optimal power flow
Power system transient stability

ABSTRACT

Multi-Contingency Transient Stability Constrained Optimal Power Flow (MC-TSCOPF) models optimize the economic dispatch of power systems while ensuring their stability after a series of reference incidents. This paper proposes a MC-TSCOPF model that represents the power balance at each node of the system and at each sample time. The proposed model includes non-linear loads, synchronous generators, a windfarm, and a Flywheel Energy Storage system (FESS). The model is written on GAMS and solved using a standard Interior Point algorithm. This study focuses on the Fuerteventura-Lanzarote insular grid in Spain, where stability problems and load shedding cause high additional costs due to the low inertia of the system. A FESS has been recently installed in the system to improve its stability, taking advantage of its high-power capacity and rapid response. The proposed TSCOPF model has been applied to optimize the operation of the FESS to support stability in the event of a contingency. The results of the study show that 1) a proper model of non-linear loads is essential in TSCOPF studies; 2) the proposed MC-TSCOPF provides a tool for minimizing the generation costs while ensuring transient and frequency stability; and 3) it is possible to further reduce the generation costs by using the proposed model to calculate an optimal dynamic response of the FESS.

Nomenclature

Indices and Sets

i, j	Index of nodes, running from 1 to $\mathcal{N}$
t	Time periods, running from 1 to $\mathcal{T}$
$\mathcal{N}$	Set of buses
$\mathcal{T}$	Set of time periods

Control variables

E_{fd}	Field voltage [p.u.]
K_{WF}	Binary variable that is equal to 1 if wind farm is connected, and 0 otherwise
P_{injFW},P_{absFW}	Injected/absorbed active power by the FESS [p.u.]
P_G,Q_g	Generator active and reactive power [p.u.]
P_{wp},Q_{wp}	Injected/absorbed power by the wind farm [p.u.]
Q_{injFW},Q_{absFW}	Injected/absorbed reactive power by the FESS [p.u.]
ΔP	Turbine governor output [p.u.]

State variables

E'_d, E'_q	Generator internal transient voltage [p.u.]
E_{FW}	Stored energy in the FESS [p.u.]
I'_d, I'_q	Generator output current components [p.u.]
I_L	Current between nodes (i,j) [p.u.]
I_{ph}	Current through IGBT converters [p.u.]
P_e	Electrical power in the rotor of the generator [p.u.]
V	Bus voltage magnitude [p.u.]
V_r,V_{ref},R_f	IEEE1 excitation system inputs [p.u.]
α	Bus voltage phase [rad]
$\Delta\omega$	Generator speed deviation [rad/s]
δ	Rotor angle [rad].
δ_{COI}	Rotor angle of the center of inertia [rad]
φ	Bus angle between current and voltage [rad]
ω_{FW}	Flywheel angular velocity [rad/s]

Parameters

* Corresponding author.
Email addresses: farredon@ing.uc3m.es (F. Arredondo); pablole@ing.uc3m.es (P. Ledesma); ecastron@ing.uc3m.es (E.D. Castronuovo)

https://doi.org/10.1016/j.ijepes.2018.06.042
Received 10 November 2017; Received in revised form 8 June 2018; Accepted 19 June 2018
Available online xxx
0142-0615/

a, b, c	Fuel cost coefficients of thermal plants
A_p, b_b, c_p	Active power coefficients of the ZIP load model
A_q, b_q, c_q	Reactive power parameters of the ZIP load model
As, Bs	Excitation system saturation coefficients
D	Damping coefficient [p.u.]
H	Inertia constant [s].
K_A,K_F,K_E	Excitation system gains [p.u.]
K_{TG}	Turbine governor gain [s]
J	Flywheel inertia constant [kg·m^2]
P_{D0},Q_{D0}	Active, reactive nominal load [p.u.]
P_{WF}^{REF}	Available wind resource p.u.]
Q_{WF}^{REF}	Wind farm reactive power reference [p.u.]
r_a	Armature resistance [p.u.]
T_A,T_F,T_E	Excitation system time constants [s]
T'_{d0}, T'_{q0}	Generator transient time constants [s]
T_{TG}	Turbine governor time constant [s]
x_d,x_q	Synchronous reactances [p.u.]
x'_d, x'_q	Transient synchronous reactances [p.u.]
Y_{ij}	Magnitude of the element (i, j) of the bus admittance matrix [p.u.]
Δt	Time step [s]
$\eta_{iny,abs}$	Performance of the synchronous machine
θ_{ij}	Phase of the element (i,j) of the bus admittance matrix [rad]
ω_{FW}^{ref}	Steady state FESs speed [rad/s]
ω_0	Frequency reference [rad/s]

Abbreviations and Acronyms

COI	Centre of Inertia
FESS	Flywheel Energy Storage System
MC	Multi-contingency
MR	Multiple Responses
OPF	Optimal Power Flow
SR	Single Response
TSCOPF	Transient Stability Constrained Optimal Power Flow

1. Introduction

Ensuring stability and reducing generation costs are essential issues in modern power systems. Transient Stability Constrained Optimal Power Flow (TSCOPF) models have emerged over the last decade as a tool to combine the economic and secure operation requirements. The TSCOPF studies include a time-domain representation of the system dynamics in the optimization problem to account for the effects that dynamic constraints have on the optimal operation.

During the last few years various approaches have been proposed to address TSCOPF [1–4]. On the one hand, evolutionary algorithm methods that use stochastic optimization algorithms [5–7] and direct methods that rely on simplified models [8,9] have been applied to reduce the size and complexity of the problem in large power systems. Other approaches have recently included the uncertainty of the renewable generation for transient stability assessment using probabilistic techniques [10,11]. On the other hand, direct discretization methods, which discretize the differential equations representing the dynamics of the system and include them in the optimization model as algebraic equations, have been applied to smaller systems [12–15].

Direct discretization methods have the advantages of including the dynamics of all the synchronous machines and using standard nonlinear programming solvers, but they are difficult to apply to large. The two main problems associated with the direct discretization TSCOPF studies is the large number of restrictions and variables and the high nonlinearity of the electromechanical oscillations between synchronous generators. The size of the model has been reduced in previous studies by representing the grid and the loads as a linear circuit and applying the Kron reduction method [12–15]. This approach has the disadvantage of representing loads as constant impedances. It is also a common practice to represent synchronous generators by using the classical model instead of a standard dynamic model in the dq-axes reference frame [12–14].

The object of this study is the insular power system of Fuerteventura-Lanzarote in Spain. The small size and low inertia of the system, which contains two conventional power plants and a wind farm, make it prone to transient and frequency stability problems. Flywheel Energy Storage Systems (FESS) have received growing interest in practical studies as a tool for increasing the stability, especially in small and isolated power systems where stability and frequency problems are major concerns. High power capacity, short access time, high efficiency, and small environmental impact make flywheels suitable for this purpose [16]. A FESS has been installed in the island of Lanzarote. This device has proven to be a useful resource to improve the frequency stability in small systems [17–19]. However, the calculation of its optimal response to a contingency has not been clearly determined in the literature.

This paper proposes a novel Multi-Contingency TSCOPF (MC-TSCOPF) model based on the direct discretization method. The aim of the study is to minimize the generation costs while ensuring stability. Instead of representing the grid as a linear passive circuit, the proposed model represents the active and reactive power injected at each node and at each sample time as independent variables. Therefore, this approach allows modelling loads as standard ZIP models instead of assuming constant impedances. Furthermore, it enables the integration of variable-speed wind farms and FESSs, represented as devices that inject power according to their control systems and independent of the magnitude of the voltage at the connection point. In the study, the synchronous generators are represented by the transient, 4th-order generator model, that provides an accurate representation for transient stability studies as stated in [9,20].

The main contributions of this paper are as follows:

- A direct discretization MC-TSCOPF model that includes non-linear loads and combines frequency and transient stability constraints.
- The integration of a FESS model into the TSCOPF problem.
- The optimization of the dynamic response of the FESS to reduce generation costs while ensuring both frequency and transient stability.

The optimization algorithm is applied to a real system in the Canary archipelago (Spain), where a FESS has been put in operation. The method proposed here is used to optimize the generation costs while ensuring stability in the event of any critical contingency. The results are compared with those obtained with the conventional operation of the FESS.

The rest of paper is organized as follows: Section 2 describes the proposed TSCOPF model, including the FESS; Section 3 describes the case study; Section 4 shows and discusses the results obtained when solving the proposed MC-TSCOPF; and Section 5 concludes the paper.

2. Description of the model

The TSCOPF models based on direct discretization are composed of two parts: the steady-state and the time-domain period. The steady-state or pre-fault stage corresponds to the normal operation of the system, and the time-domain period simulates the behaviour of the system during and after a contingency. The time-domain period is subdivided

into fault and post-fault stages. All periods are included as equality and inequality constraints and solved in the same optimization problem. This section gives a complete account of the steady-state and time-domain equations of the proposed TSCOPF model, organized according to the parts and components that compose the power system.

2.1. Grid model

The power balance at each bus and at each sample time is represented by the following general equations:

$$\begin{aligned} & I_{di}^{t}V_i^t\sin(\delta_i^t-\alpha_i^t)+I_{qi}^{t}V_i^t\cos(\delta_i^t-\alpha_i^t) \\ & -P_{D0,i}(A_{p,i}+B_{p,i}V_i^t+C_{p,i}(V_i^t)^2) \\ & +P_{injFW,i}^{t}-P_{absFW,i}^{t}+P_{WP,i}^{t} \\ & -V_i^t\sum_{\forall j}V_j^tY_{ij}\cos(\alpha_i^t-\alpha_j^t-\theta_{ij})=0 \end{aligned} \tag{1}$$

$$\begin{aligned} & I_{di}^{t}V_i^t\cos(\delta_i^t-\alpha_i^t)-I_{qi}^{t}V_i^t\sin(\delta_i^t-\alpha_i^t) \\ & -Q_{D0,i}(A_{q,i}+B_{q,i}V_i^t+C_{q,i}(V_i^t)^2) \\ & +Q_{injFW,i}^{t}-Q_{absFW,i}^{t}+Q_{WP,i}^{t} \\ & -V_i^t\sum_{\forall j}V_j^tY_{ij}\sin(\alpha_i^t-\alpha_j^t-\theta_{ij})=0 \end{aligned} \tag{2}$$

The first two terms in (1) and (2) represent the power injected by a synchronous generator, if connected to the bus. The terms containing P_{D0} and Q_{D0} Q_{D0} represent loads consisting of a constant power, a constant current, and a constant impedance component (ZIP model). The terms P_{absFW},P_{inyFW},Q_{absFW}, and Q_{inyFW} represent the power absorbed or injected by any FESS connected to the bus. The power injected by a wind farm is modelled by P_{WF} and Q_{WF}, respectively.

The power plant generation limits, current limits in lines and transformers, and voltage magnitude limits at the pre-fault stage are represented by (3), (4), and (5) respectively.

$$\left\{P_{Gi}^{MIN};Q_{Gi}^{MIN};0\right\}\leqslant\left\{P_{Gi}^{0};Q_{Gi}^{0};I_{L,ij}^{0}\right\}\leqslant\left\{P_{Gi}^{MAX};Q_{Gi}^{MAX};I_{L.ij}^{MAX}\right\} \tag{3}$$

$$\begin{aligned} & I_{L,ij}^2-Y_{ij}^2\left(V_i^0\cos\alpha_i^0-V_j^0\cos\alpha_j^0\right)^2 \\ & -Y_{ij}^2\left(V_i^0\sin\alpha_i^0-V_j^0\sin\alpha_j^0\right)^2=0 \end{aligned} \tag{4}$$

$$\left\{V_i^{MIN}\right\}\leqslant\left\{V_i^0\right\}\leqslant\left\{V_i^{MAX}\right\} \tag{5}$$

Eqs. (1) and (2) are included both in the steady-state stage and in each interval of the time-domain period. Eqs. (3)–(5) are only present in the steady-state stage.

2.2. Power plant model

Eqs. (6)–(14) represent the well-known, 4th-order transient synchronous generator model [21], whose state variables are the d-q components of the internal voltage, the rotor speed deviation and the rotor angular deviation. Eqs. (6)–(9) are the result of applying the trapezoidal rule to discretize the differential equations of the model, and Eqs. (10)–(13) define the initial values of the state variables. Eq. (14) limits the field voltage in the pre-fault stage.

$$\begin{aligned} & E_{di}^{\prime t+1}\left(1+\Delta t/2T_{q0i}^{\prime}\right)-E_{di}^{\prime t}\left(1-\Delta t/2T_{q0i}^{\prime}\right) \\ & -\left(\Delta t/2T_{q0i}^{\prime}\right)\left(x_{qi}-x_{qi}^{\prime}\right)\left(I_{qi}^{t+1}+I_{qi}^{t}\right)=0 \end{aligned} \tag{6}$$

$$\begin{aligned} & E_{qi}^{\prime t+1}(1+\Delta t/2T_{d0i}^{\prime})-E_{qi}^{\prime t}\left(1-\Delta t/2T_{d0i}^{\prime}\right) \\ & -\left(\Delta t/2T_{d0i}^{\prime}\right)\left[E_{fdi}^{t+1}+E_{fdi}^{t}\right. \\ & \left.-(x_{di}-x_{di}^{\prime})(I_{di}^{t+1}+I_{di}^{t})\right]=0 \end{aligned} \tag{7}$$

$$\begin{aligned} & \Delta\omega_i^{t+1}\left(1+D_i\Delta t/4H_i\right) \\ & -\Delta\omega_i^{t}\left(1-D_i\Delta t/4H_i\right)-\left(\Delta t/4H_i\right)\left(2P_{mi}\right. \\ & \left.+\Delta P_i^{t+1}+\Delta P_i^{t}-P_{ei}^{t+1}-P_{ei}^{t}\right)=0 \end{aligned} \tag{8}$$

$$\delta_i^{t+1}-\delta_i^t-(\Delta t/2)\omega_0(\Delta\omega_i^{t+1}+\Delta\omega_i^t)=0 \tag{9}$$

$$E_{di}^{\prime 0}-(x_{qi}-x_{qi}^{\prime})I_{qi}^{0}=0 \tag{10}$$

$$E_{qi}^{\prime 0}+(x_{di}-x_{di}^{\prime})I_{di}^{0}-E_{fdi}^{0}=0 \tag{11}$$

$$P_{mi}-P_{ei}^{0}=0 \tag{12}$$

$$\Delta\omega_i^0=0 \tag{13}$$

$$E_{fdi}^{MIN}\leqslant E_{fdi}^{0}\leqslant E_{fdi}^{MAX} \tag{14}$$

Eq. (15) calculates the active power output of the synchronous machines and Eqs. (16) and (17) relate the internal variables of the synchronous machine with the variables in the generation bus, at each time step of the time-domain period. Eqs. (18) and (19) calculate the active and reactive power produced by the power plants in the steady-state stage.

$$P_{ei}^{t}-E_{di}^{\prime t}I_{di}^{t}-E_{qi}^{\prime t}I_{qi}^{t}=0 \tag{15}$$

$$V_i^t\sin(\delta_i^t-\alpha_i^t)-E_{di}^{\prime t}+r_{ai}I_{di}^{t}-x_{qi}^{\prime}I_{qi}^{t}=0 \tag{16}$$

$$V_i^t\cos(\delta_i^t-\alpha_i^t)-E_{qi}^{\prime t}+r_{ai}I_{qi}^{t}+x_{di}^{\prime}I_{di}^{t}=0 \tag{17}$$

$$P_{Gi}^{0}-I_{di}^{0}V_i^0\sin(\delta_i^0-\alpha_i^0)-I_{qi}^{0}V_i^0\cos(\delta_i^0-\alpha_i^0)=0 \tag{18}$$

$$Q_{Gi}^{0}-I_{di}^{0}V_i^0\cos(\delta_i^0-\alpha_i^0)+I_{qi}^{0}V_i^0\sin(\delta_i^0-\alpha_i^0)=0 \tag{19}$$

Eqs. (20)–(25) represent the excitation system in each time step of the time-domain period, modelled as an IEEE Type 1 exciter [21]. Eqs. (20)–(22) result from the discretization of the corresponding differential equations, and Eqs. (23)–(25) define the initial values of the state variables. Eqs. (26) and (27) represent the saturation of the amplifier in the excitation system.

$$E_{fdi}^{t+1}(1+(K_{ei}\Delta t/2T_{Ei})) - E_{fdi}^{t}(1-(K_{ei}\Delta t/2T_{Ei})) + ((E_{fdi}^{t+1}A_{s,i}e^{B_{s,i}E_{fdi}^{t+1}} + E_{fdi}^{t}A_{s,i}e^{B_{s,i}E_{fdi}^{t}})\Delta t)/2T_{Ei} - \Delta t(Vr_i^{t+1}+Vr_i^{t})/2T_{Ei} = 0 \quad (20)$$

$$(Vr_{aux,i}^{t+1}/K_{Ai})(2T_{Ai}/\Delta t+1) - (Vr_i^{t}/K_{Ai})(2T_{Ai}/\Delta t-1) - R_{Fi}^{t+1} + R_{Fi}^{t} - (K_{Fi}/T_{Fi})(E_{fdi}^{t+1}+E_{fdi}^{t}) - (V_i^{t+1}+V_i^{t}) + 2V_{ref,i} = 0 \quad (21)$$

$$R_{Fi}^{t+1}(1+\Delta t/2T_{Fi}) - R_{Fi}^{t}(1-(\Delta t/2T_{Fi})) - (\Delta tK_{Fi}/T_{Fi}^{2})(E_{fdi}^{t+1}+E_{fdi}^{t}) = 0 \quad (22)$$

$$-(K_{ei}+A_{s,i}e^{Bs_{,i}E_{fdi}^{0}}))E_{fdi}^{0}+Vr_i^{0}=0 \quad (23)$$

$$-Vr_i^{0}+K_{Ai}(R_{Fi}^{0}-(K_{Fi}/T_{Fi})E_{fdi}^{0}+V_{refi}-V_i^{0})=0 \quad (24)$$

$$-R_{Fi}^{0}-(K_{Fi}/T_{Fi})E_{fdi}^{0}=0 \quad (25)$$

$$Vr_{aux1,i}^{t+1}=\max(Vr_i^{\min},Vr_{aux,i}^{t+1}) \quad (26)$$

$$Vr_i^{t+1}=\min(Vr_i^{\max},Vr_{aux1,i}^{t+1}) \quad (27)$$

Finally, the turbine governor is represented by (28) and (29) as a first-order control loop [15].

$$\Delta P_i^{t+1}(1+\Delta t/2T_{TGi}) - \Delta P_i^{t}(1-\Delta t/2T_{TGi}) + (\Delta t/2T_{TGi})(\Delta\omega_i^{t+1}+\Delta\omega_i^{t})=0 \quad (28)$$

$$\Delta P_i^{0}=0 \quad (29)$$

Eqs. (10)–(14), (18), (19), (23)–(25), and (29) are included in the pre-fault stage and initialize the dynamic algebraic equations of the power plant. Eqs. (6)–(9), (20)–(22), and (28) are the dynamic algebraic equations represented in the time-domain period. Auxiliary Eqs. (15)–(17) are included both in the steady-state stage and in each interval of the time-domain period.

2.3. FESS model

Energy Storage Systems are increasingly used in power systems to increase the penetration of renewable energies and improve the dynamic stability [17]. In particular, FESS have received growing interest as a tool to improve transient and frequency stability [17,18] because of their high power capacity and fast response. A FESS consists of a rotating mass or flywheel where energy is stored mechanically as kinetic energy. An integrated synchronous machine converts the energy from mechanical into electrical or vice versa, thus enabling the exchange of power between the flywheel and the power system [22]. Back-to-back IGBT converters act as an interface between the FESS and the grid, allowing the spinning mass to rotate at a variable speed [23], Fig. 1.

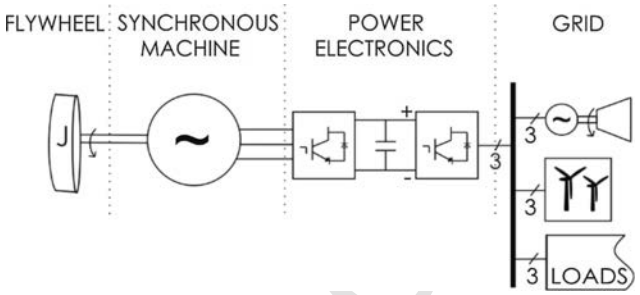

Fig. 1. FESS connected to the grid.

A FESS is a device capable of exchanging active and reactive power independently, since it is connected to the network through electronic power converters. The main control strategies for FESS are: 1) Improvement of frequency and transient stability by means of injecting or absorbing active power to/from the network; and 2) Voltage support by means of reactive power control. As the objective of this work is the improvement of transient and frequency stability, the value of the reactive power is set to zero.

The Fuerteventura-Lanzarote power system includes a FESS [24] that is primarily used to stabilize the frequency. Given that the time response of the FESS is small compared to the time scale of the transient stability studies, the FESS is represented in the TSCOPF model as a source of active power. Eq. (30) represents the relation between the stored energy in the FESS (E_{FW}), the power injected to the grid (P_{inj}^{t+1}), the power absorbed from the grid (P_{abs}^{t+1}), and the losses ($P_{Losses,mec}^{t+1}$ and $P_{Losses,IGBT}^{t+1}$). Parameters η_{inj} and η_{abs} represent the efficiency of the synchronous machine as it injects energy to, or extracts energy from the grid. Mechanical losses ($P_{Losses,mec}^{t+1}$) are defined in (31) as a combination of axial rotating and windage losses [25]. Eq. (32) represents the losses in the electronic converters ($P_{Losses,IGBT}^{t+1}$), modelled as a function of the magnitude of the current through the IGBT converters [26,27]. When FESS internal losses can be neglected, parameters a_{rt}, b_{rt}, and c_{rt} (31) a_{conv}, b_{conv}, and c_{conv} (32) can be considered zero.

$$E_{FW}^{t+1}=E_{FW}^{t}+\Delta t\left[P_{absFW}^{t+1}\eta_{abs}-P_{injFW}^{t+1}/\eta_{inj}-P_{Losses,mec}^{t+1}-P_{Losses,IGBT}^{t+1}\right] \quad (30)$$

$$P_{Losses,mec}^{t+1}=a_{rt}\omega_{FW}^{t+1}+b_{rt}\left(\omega_{FW}^{t+1}\right)^{2}+c_{rt}\left(\omega_{FW}^{t+1}\right)^{2} \quad (31)$$

$$P_{Losses,IGBT}^{t+1}=a_{conv}+b_{conv}I_{ph}^{t+1}+c_{conv}(I_{ph}^{t+1})^{2} \quad (32)$$

Eqs. (33) and (34) calculate the speed of the rotating mass and the magnitude of the current through the electronic converters, respectively. Eq. (35) specifies the initial amount of stored energy in the FESS, here, 80% of its maximum capacity. The power provided by the FESS in the steady state stage is initialized in (36). Finally, limits on the FESS power and stored energy at each sample time are represented in (37). Eqs. (30)–(34) are included in each time step of the time-domain period.

$$(\omega_{FW}^{t+1})^{2}=2(E_{FW}^{t+1})^{2}/J+(\omega_{FW}^{MIN})^{2} \quad (33)$$

$$I_{ph}^{t+1}=(P_{abs}^{t+1}+P_{iny}^{t+1})/(\sqrt{3}U^{t+1}) \quad (34)$$

$$E_{FW}^{0}=0.8E_{FW}^{MAX} \quad (35)$$

$$\{P^0_{inyFW};P^0_{absFW}\} = \{0;0\} \tag{36}$$

$$\{0;0;\omega^{MIN}_{FW}\} \leqslant \{P^t_{inyFW};P^t_{absFW};\omega^t_{FW}\} \leqslant \{P^{MAX}_{iny};P^{MAX}_{abs};\omega^{MAX}_{FW}\} \tag{37}$$

2.4. Wind farm model

The variable speed wind farm is modelled as a constant power source with a constant power factor. Fault ride-through requirements for wind farms published in the Spanish national grid code by the Transmission System Operator [28] are applied. Therefore, the wind farm is disconnected when a voltage dip at the wind farm connection point exceeds the low voltage ride-through limits.

$$P^t_{WP} = K^t_{WF} P^{ref}_{WF} \tag{38}$$

$$Q^t_{WP} = K^t_{WF} Q^{ref}_{WF} \tag{39}$$

$$pf = P^{ref}_{WF}/Q^{ref}_{WF} \tag{40}$$

$$K^0_{WF} = 1 \tag{41}$$

Eqs. (38) and (39) calculate the active and reactive power injected to the grid at each sample time *t*, respectively. The parameter P^{ref}_{WF} represent the available wind resource. Eq. (40) calculates the reactive power Q^{ref}_{WF} that depends on the control strategy, in this case power factor control. The binary variable K^t_{WF} defines whether the plant is connected or disconnected. During the pre-fault stage, the plant is connected and therefore takes the value of 1, as shown in (41). During the fault and post-fault stages, if the voltage is lower than a certain limit then the windfarm is disconnected and K^t_{WF} is zero.

2.5. Transient and frequency stability criteria

Transient and frequency stability dynamic constraints are both important in the Fuerteventura-Lanzarote power system. The transient stability constraint is modelled as a limit on the deviation of the rotor angles of the synchronous machines with respect to the centre of inertia (COI), as defined in (42) and (43). The frequency stability criterion is implemented as a limit on the rotor speed of the synchronous generators, as shown in (44).

$$\delta^t_{COI} - \sum_i H_i \delta^t_i \Big/ \sum_i H_i = 0 \tag{42}$$

$$-\delta^{MAX} \leqslant \delta^t_i - \delta^t_{COI} \leqslant \delta^{MAX} \tag{43}$$

$$-\Delta\omega^{MIN}_i \leqslant \Delta\omega^t_i \leqslant \Delta\omega^{MAX}_i \tag{44}$$

2.6. Objective function of the TSCOPF

The objective function is:

$$\begin{aligned} \text{Min. } & f\left(P^0_{Gi}, \omega^t_{FW}, P^t_{absFW}\right) \\ &= \sum_{i=1}^{i=N} a_i P^{0^2}_{Gi} + b_i P^0_{Gi} + c_i \\ &\quad + \sum_{t=0}^{t=T} \left[a_{FW}(\omega^t_{FW} - \omega^{ref}_{FW})^2 + b_{FW} P^t_{absFW}\right] \end{aligned} \tag{45}$$

The first term in (45) represents the generation cost as a quadratic function of the power produced by the conventional power plants. The second term in (45) is introduced to ensure that the solution of the TSCOPF model produces a smooth dynamic response of the FESS. The minimization of the mean squared error of the FESS speed with respect to the reference speed has the effect of rapidly restoring the FESS speed to the specified steady state value. This readies the FESS to act in case of another contingency. Finally, the power absorbed by the FESS is slightly penalized by b_{FW} to ensure a unique solution of P_{absFW} and P_{inyFW}. The parameters a_{FW} and b_{FW} are purposely small, to ensure that the second term in (45) is significantly smaller than the first term and has a negligible effect on the final value of the objective function.

2.7. Multi-contingency formulation

The proposed TSCOPF as described in (1)–(45) models a single contingency. However, system operators often identify a set of critical incidents that may result in a loss of stability. Therefore, the model has been extended to include a set of reference incidents. The resulting MC-TSCOPF model is built by keeping the equations that correspond to the pre-fault stage, and repeating equations, (1)–(2), (6)–(9), (15)–(17), (20)–(27), (28), (38)–(39) and (42)–(44) once for every incident. Eqs. (30)–(34) and (37), which represent the dynamic response of the FESS, can be kept unique to model a single response of the FESS to all incidents or repeated for every contingency to model a different response of the FESS to each incident. Both alternatives are discussed in Section 4.

2.8. Software implementation

The proposed model is implemented in a software framework that automatically builds and solves it. A Python program reads the parameters of the power system from a standard PSSE file, together with information about the contingencies and the stability limits, and writes the complete model in the GAMS language. The model is then fed into GAMS and solved using the interior point algorithm IPOPT. This approach facilitates the application of the TSCOPF model to different cases and solvers. The procedure is described in detail in [15].The accuracy of the model has been verified using time-domain simulations with PSSE.

3. Study case

The Spanish islands of Lanzarote and Fuerteventura in the Canary archipelago, are located in the Atlantic Ocean off the coast of Northern Africa. Fig. 2 shows the 66 kV transmission system, which includes a submerged AC cable between the islands. The topology of the system is mostly linear, apart from a single mesh in the northern area, where most of the load is located.

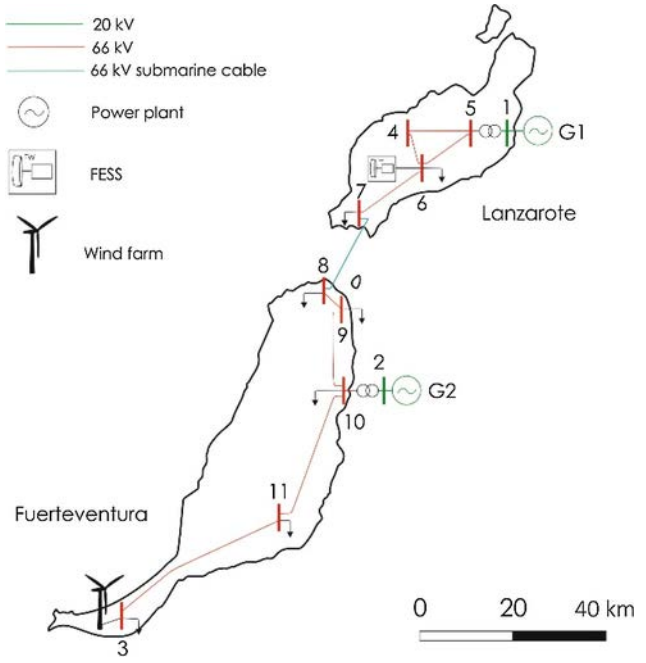

Fig. 2. Lanzarote-Fuerteventura power system.

Generation is provided by two power plants connected to buses 1 and 2 in the North and Centre of the system, with maximum capacities 187 and 159 MW, respectively, and by a 12 MW wind farm in the South. Regular winds from the Atlantic Ocean provide a relatively steady production of wind power. The fuel cost coefficients of power plants G1 and G2 are considered linear with values of 20 and 50 €/MWh, respectively. The operation cost of the wind generation is considered 10 €/MWh. In the present study, all parameters are considered known. When uncertainties in loads, wind power generation, generation costs and equipment availability are considered in the system [10,11], the proposed optimization problem can be applied to the most probable values of the parameters, following Monte Carlo or other approaches.

A 1.65 MW FESS is currently connected to bus 6, which is close to generator G1 and to the main urban area in the system. Given the plans to increase the capacity of the FESS in the near future due to the positive effects of its actuation in several real cases, a 5 MW FESS is modelled in the study. A set of reference incidents that can result in the loss of transient and/or frequency stability are specified based on the experience and knowledge of the system. These reference incidents are 1) a direct three-phase short-circuit at bus 5, cleared by a back/up protection after 300 ms; 2) a direct three-phase short-circuit at bus 8, cleared by a back/up protection after 300 ms; 3) a loss of the largest load, which is the load connected at bus 6; and 4) a loss of the wind farm.

4. Results and discussion

4.1. Effect of load modeling on the results of the TSCOPF

Load modelling has a substantial impact on the results of the transient stability simulations and must therefore be properly accounted for in the TSCOPF models. ZIP load models, which calculate the load as a quadratic function of the voltage, are a standard in power system dynamic simulations [29,30]. However, the common practice in TSCOPF studies that include all dynamic equations in the optimization model has been to represent loads as constant impedances to reduce the number of equations [31]. The proposed TSCOPF model represents the injected power at each bus as an independent variable at every sample time, thus making it possible to introduce the ZIP loads in (1) and (2).

To evaluate the effects that load modelling has on the TSCOPF, the same fault has been studied using a linear load model and a ZIP model consisting of a 40% constant impedance, 30% constant current and 30% constant power. The studied fault is the short circuit at bus 5, which is the most severe of the reference incidents listed in Section 3.

The TSCOPF using the ZIP load model results in a generation cost of 6476 €, that is 190 € (3%) more expensive than the dispatch obtained using the linear load model. Fig. 3 shows the bus voltages as provided by both load models. The ZIP load model produces larger oscillations and results in a more conservative dispatch. It can be concluded that the non-linear nature of loads must be preserved in order to ensure that the solution is transiently stable.

4.2. Optimal FESS response to support transient stability

The usual actions performed by FESSs to stabilize the frequency in small power systems are to inject active power when the frequency decreases and to consume active power when the frequency increases [18,19]. The selection of a FESS strategy to support transient stability is not as straightforward because it depends on several factors, such as the location of the flywheel within the system, the operating point, and the type and location of the fault. The integration of the FESS model into the TSCOPF, as defined by Eqs. (30)–(37), makes it possible to optimize the dynamic response of the flywheel and thereby minimize the generation costs while ensuring transient stability.

Fig. 4 shows the results provided by the TSCOPF when the transient stability constraints are applied. On the one hand, Fig. 4a) shows the rotor angles of the generators, together with the stored energy in the FESS. On the other hand, Fig. 4b) shows the power delivered to the system by the conventional power plants, together with the power exchanged between the FESS and the network. The case corresponds to a short-circuit at bus 5, cleared by a backup protection after 300 ms. The rotor angles are constrained within the COI angle ±60° by (43), but the

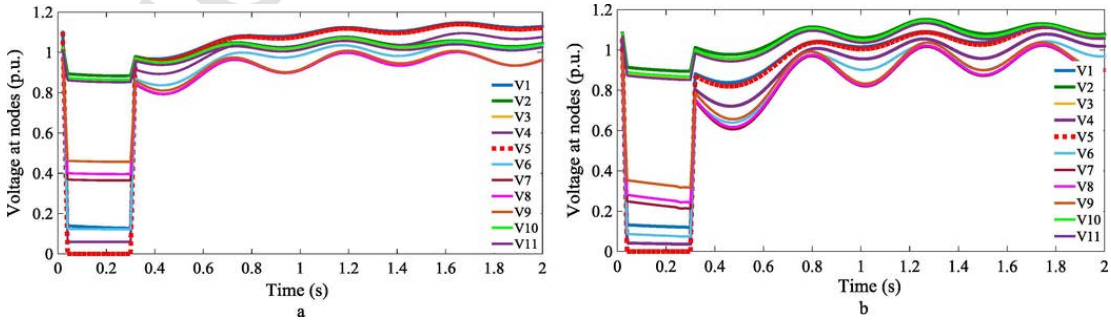

Fig. 3. Effect of the load model on the TSCOPF solution. a) Constant impedance load model and b) ZIP load model.

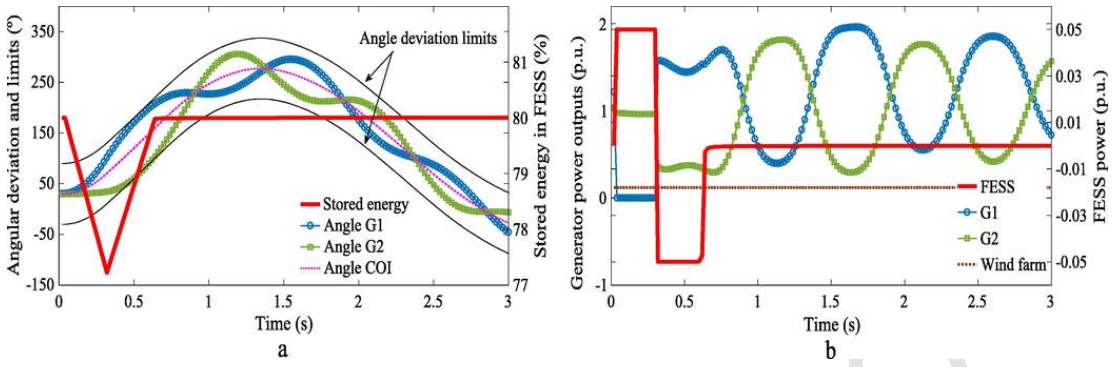

Fig. 4. TSCOPF model with transient stability constraints: a) Rotor angle of generators and energy stored in the FESS; b) Power output of generators and FESS.

frequency constraints in (44) are not applied. It can be seen in Fig. 4a) that both generators reach the maximum angle deviation limits, approximately 0.5 s, after the fault. During the fault, generator G1 cannot deliver power to the system and accelerates, whereas generator G2 continues delivering power, as shown in Fig. 4b). The FESS reacts by injecting power to accelerate the system and reduce the angle deviation between G1 and G2. Once the fault is cleared, the FESS consumes power to decelerate generator G1, to which it is electrically near, thereby reducing its oscillation with respect to generator G2.

It can be seen in Fig. 4a) that the energy stored in the FESS returns to its initial value once there is no action required from the flywheel to stabilize the system. This is due to the component of the objective function that is linked to the speed deviation.

It is remarkable that the FESS initially injects power as the frequency is rising, which is contrary to the typical response of FESS controls to support frequency stability. Conventional frequency FESS controls in this particular case are contrary to the optimal behaviour and can have a destabilizing effect.

4.3. Optimal FESS response to support transient and frequency stability

Frequency stability is a concerning issue in island power systems because the relatively small inertia makes it difficult to maintain the frequency within acceptable limits after severe losses of generation or load. Fig. 5 shows the results obtained when the frequency constraint (44) is included in the model and the frequency deviation is constrained between −0.02 p.u. (49 Hz) and 0.04 p.u. (52 Hz). The minimum frequency is set to 49 Hz because it is the value at which the under-frequency load shedding scheme begins. The fault is the same as in the previous case: a short-circuit at bus 5 cleared after 300 ms.

Fig. 5a) shows that generator G1, which is close to the fault, accelerates quickly during the short-circuit because the active power that the synchronous generator cannot inject into the system is transformed into kinetic energy. Once the fault is cleared, generators G1 and G2 oscillate but retain their synchronism. The solution of the optimization model transfers some generation from G1 to G2 to ensure that the angular deviation between the generator remains within the limits. It can be seen that the lower limit is nearly reached by G2 approximately at time = 0.5 s. The energy stored in the FESS varies as the FESS injects and consumes power, but remains always within the limits.

Fig. 5b) shows the rotor speeds of the synchronous machines, together with the power exchanged between the FESS and the network. Here it can be seen again the acceleration of G1 during the fault, and the oscillations between G1 and G2 once the fault is cleared. The solution of the optimization model modulates the power injected by the FESS to maintain the speed of G1 and G2 over the limits. It can be seen that generator G2 reaches the lower limit at, approximately, time = 2.2 s.

Overall, the pattern of the power injected by the FESS, shown in Fig. 5b), is more complex than in the previous case, and responds to two combined effects. On the one hand, positive and negative injections alternate during the first 1.5 s to damp the electromechanical oscillations between the generators. On the other hand, a net positive amount of energy is injected before the minimum frequency limit is reached to reduce the frequency drop. Once there is no action of the FESS required to recover the system, the FESS absorbs energy to return to its initial state due to the component linked to the deviation of the speed in the objective function. It is remarkable that the rapid response of the controls of the FESS makes it possible to combine a response with positive and negative exchanges of active power, as shown in Fig. 5b), damping the electromechanical oscillations between synchronous generators and leading the system to a more stable operation.

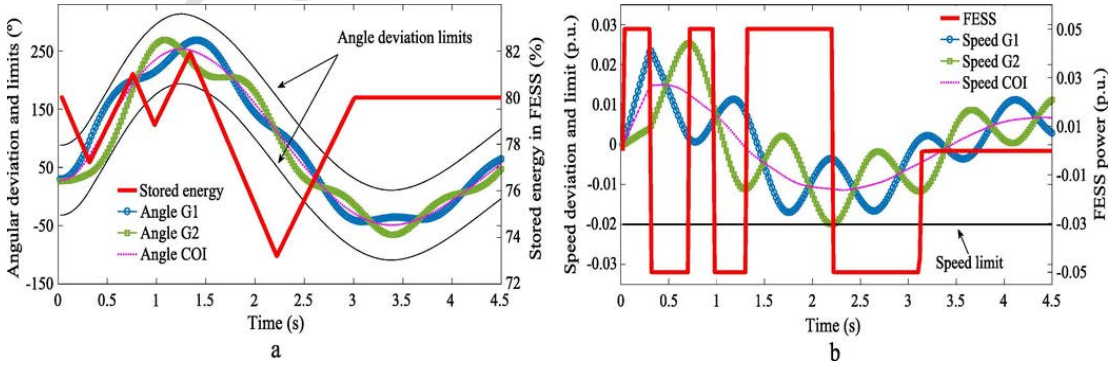

Fig. 5. TSCOPF model with transient stability and frequency constraints: a) Rotor angle of generators and energy stored in the FESS; b) Speed deviation of generator and power output of FESS.

4.4. Economic assessment considering one contingency

This section analyses the economic cost of ensuring that the system remains stable and no load is shed after any of the reference incidents. Three cases are considered: a) without the flywheel energy storage system (NO FESS); b) with a conventional control in which the flywheel injects or absorbs fixed values of power following frequency deviations, as described in [18,19] (C-FESS); and c) optimizing the dynamic response of the flywheel with the proposed TSCOPF (O-FESS). The results are compared with a classical OPF without dynamic constraints.

The solution for a classical OPF results in a generation cost of 5549 €, with G1 generating 157.8 MW and G2 generating 45.5 MW, as shown in the first row of Table 1. The remaining rows correspond to the critical reference incidents defined in Section 3. Total cost includes the variable operation costs of wind generation [32]. Both the rotor angle constraints and the frequency constraints are included in the model. It can be seen in Table 1 that the largest cost is reached in the case of a short-circuit at bus 5, which is a consequence of bus 5 being in proximity to G1, the largest and most economical plant. Application of the TSCOPF model shows that the total generation cost increases with respect to the OPF by 16.7% (927 €) when there is no FESS, and by 15.3% (850 €) when the FESS is connected and a conventional control is applied. The optimized control of the FESS makes it possible to further reduce the cost to 6166 €, only 13.3% (737 €) above the cost of the solution provided by the OPF.

The results obtained when a short-circuit is applied at bus 8 are qualitatively similar, although the introduction of the dynamic constraints results in lower costs because the incident is less critical. The total cost increases with respect to the OPF by 1.3% (70 €) when there is no FESS, by 1.1% (59 €) when the FESS is connected and a conventional control is applied, and by 1.01% (55 €) when the control of the FESS is optimized.

The dynamic constraints after the loss of load incident cause an incremental increase of 2.2% for the cost when there is no FESS, but this cost is eliminated when the FESS is connected and either a conventional or optimized control is applied. Finally, the dynamic constraints do not increase the cost after the disconnection of the wind farm, which can be explained by the relatively small size of the wind farm that does not compromise the stability of the system.

Table 1
Results of TSCOPF considering one incident at a time.

	FESS control	G1 (MW)	G2 (MW)	Cost (€)	ΔCost (%)
OPF	Do not apply	157.8	45.5	5549	0
SC at bus 5	NO FESS	106.4	84.6	6476	16.7
	C-FESS	108.8	82.1	6399	15.3
	O-FESS	112.5	78.3	6286	13.3
SC at bus 8	NO FESS	144.6	52.1	5619	1.3
	C-FESS	145.8	51.4	5608	1.1
	O-FESS	146.1	51.3	5604	1.0
Loss of load	NO FESS	169.5	43.2	5669	2.2
	C & O-FESS	157.8	45.5	5549	0
Loss of WF	All cases	157.8	45.5	5549	0

The proposed TSCOPF is also evaluated in a modified IEEE 57 Bus Test System [33] that includes wind power generation and a FESS. The size and location of the wind farms can be found in Table 7. The FESS is located at bus number 15, near to the main generation area. Table 2 presents the solution of the TSCOPF model when a short-circuit is applied at bus number 1. Three cases of study are evaluated: a) without flywheel (NO FESS); b) considering the optimal response of a flywheel of 10 MW (O-FESS 10 MW); and c) considering the optimal response of a flywheel of 20 MW (O-FESS 20 MW).

The results in Table 2 show that the response of the FESS tends to reduce the generation costs because it improves the stability to the system, making it possible to shift generation to power plants that are more economical. The effect is more pronounced as the size of the FESS increases.

4.5. Economic assessment considering multiple contingencies

The optimal operation of the FESS corresponding to one contingency can aggravate the effect of another contingency. The MC-TSCOPF model makes it possible to calculate the most economical operation point that ensures a stable operation and avoids load shedding after any of the reference incidents. The MC-TSCOPF is applied to the power system of Fuerteventura-Lanzarote. The results of the MC-TSCOPF, which includes all critical contingencies in Table 1, are presented in Table 3. The first row corresponds to a case that does not include the FESS. In this case, the dynamic constraints increase the generation cost by 21.2% with respect to the OPF.

The second row represents a case in which the FESS is connected but its dynamic response is not optimized. Here, the cost is improved with respect to the previous case. The third row corresponds to a case that applies a single common FESS response (SR) to every incident. It is noted that the implementation of this method requires that the FESS control system detects that an incident has occurred in the grid. The cost is further improved with respect to the previous cases.

The final case considers multiple FESS responses (MR), which means that there is a different response for each incident. The implementation of this strategy requires that the FESS control system be aware of the type of incident that has occurred. The resulting generation cost is slightly lower than in the case of the SR.

5. Conclusion

A direct discretization MC-TSCOPF model that facilitates the inclusion of renewable generation, an energy storage system, and non-linear loads is formulated. The application of the proposed MC-TSCOPF model to the Fuerteventura-Lanzarote island system provides the opportunity to calculate an optimal dispatch that ensures the system remains stable and no loads are shed after any one of a set of predefined reference incidents.

The integration of an FESS model in the MC-TSCOPF problem can be used to optimize the dynamic response of the flywheel to support transient and frequency stability. Ensuring the stability in electric

Table 2
Results of TSCOPF on the dispàtch of the IEEE 57 Bus Test System.

	G1 (MW)	G2 (MW)	G3 (MW)	G4 (MW)	G5 (MW)	G6 (MW)	G7 (MW)	Cost (M.U.)
NO FESS	226.5	239.5	500	11.6	20.7	20.8	39	33,820
O-FESS 10 MW	226.9	240.7	500	10.9	19.9	21	38.8	33,791
O-FESS 20 MW	227	242.1	500	10.6	19	20.9	38.7	33,764

Table 3
Results of MC-TSCOPF including all reference incidents.

	G1 (MW)	G2 (MW)	Cost (€)	ΔCost (%)
MC-TSCOPF	101.7	91.5	6726	21.2
MC-TSCOPF + C-FESS	105.1	86	6524	17.6
MC-TSCOPF + O-FESS SR	111.7	79.3	6317	13.8
MC-TSCOPF + O-FESS MR	112.5	78.3	6286	13.3

power systems presents additional costs because in some cases it entails to shift generation to power plants that are more expensive. The inclusion of the FESS dynamic response in the MC-TSCOPF model allows the generation costs to be reduced while ensuring stability after any of the reference incidents. It is found that the optimal response of the flywheel after a short-circuit may be contrary to the response of conventional FESS controls.

Acknowledgements

Francisco Arredondo acknowledges the University Carlos III of Madrid (Ayudas para la Movilidad del Programa Propio de Investigación).

Table 4
Parameters of lines and transformers of the Fuerteventura-Lanzarote power system.

Branch	R [p.u.]	X [p.u.]	B [p.u.]
1–5	0	0.02	0
2–10	0	0.02	0
4–5	0.0473	0.1515	0.0050
4–6	0.0929	0.2975	0.0098
5–6	0.0506	0.1619	0.0053
6–7	0.0895	0.2865	0.0051
7–8	0.0151	0.0323	0.0578
8–9	0.0202	0.0648	0.0021
9–10	0.1331	0.4260	0.0141
10–11	0.1687	0.5399	0.0179
3–11	0.1365	0.4370	0.0145

Table 5
Parameters of power plants and controls of the Fuerteventura-Lanzarote power system.

K_A	400	V_r^{MAX}	−7.3 p.u.	H	3 s
K_F	0.03	V_r^{MIN}	7.3 p.u.	D	2
K_E	1	As	0.09826	r_a	0 p.u.
T_A	0.02 s	Bs	0.5527	x_d, x_q	1.5 p.u.
T_F	1 s	K_{TG}	50	x'_d, x'_q	0.3 p.u.
T_E	0.8 s	T_{TG}	3 s	$T'_{d0}; T'_{q0}$	6; 1 s

Table 6
FESS parameters.

ω_{FW}^{MIN}	30	ω_{FW}^{MAX}	60	J	1333.33

Table 7
Wind power generation data from the IEEE 57 modified Bus Test System.

Units	Location (buses)	P_{WF} (MW)	Q_{WF} (Mvar)	Total Generation (MW)/(Mvar)
5	7, 21, 24, 34, 37	50	10	250/50

The values of a_{FW} and b_{FW} are 1e − 03 and 1e − 04, respectively.

Appendix

See Tables 4–7.

References

[1] S. Abhyankar, G. Geng, M. Anitescu, X. Wang, V. Dinavahi, Solution techniques for transient stability-constrained optimal power flow – Part I, IET Gener Transm Distrib 11 (12) (2017) 3177–3185.
[2] G. Geng, S. Abhyankar, X. Wang, V. Dinavahi, Solution techniques for transient stability-constrained optimal power flow – Part II, IET Gener Transm Distrib 11 (12) (2017) 3186–3193.
[3] F. Capitanescu, et al., State-of-the-art, challenges, and future trends in security constrained optimal power flow, Electr Power Syst Res 81 (8) (2011) 1731–1741.
[4] Xu Y, Dong ZY, Xu Z, Zhang R, Wong KP. Power system transient stability-constrained optimal power flow: a comprehensive review. In: *2012 IEEE Power and Energy Society General Meeting*, 2012, p. 1–7.
[5] S.W. Xia, B. Zhou, K.W. Chan, Z.Z. Guo, An improved GSO method for discontinuous non-convex transient stability constrained optimal power flow with complex system model, Int J Electr Power Energy Syst 64 (2015) 483–492.
[6] R. Ardeshiri Lajimi, T. Amraee, A two stage model for rotor angle transient stability constrained optimal power flow, Int J Electr Power Energy Syst 76 (2016) 82–89.
[7] Y. Xu, Z.Y. Dong, K. Meng, J.H. Zhao, K.P. Wong, A hybrid method for transient stability-constrained optimal power flow computation, IEEE Trans Power Syst 27 (4) (2012) 1769–1777.
[8] R. Zarate-Minano, T. Van Cutsem, F. Milano, A.J. Conejo, Securing transient stability using time-domain simulations within an optimal power flow, IEEE Trans Power Syst 25 (1) (2010) 243–253.
[9] X. Tu, L. Dessaint, I. Kamwa, A global approach to transient stability constrained optimal power flow using a machine detailed model, Can J Electr Comput Eng 36 (1) (2013) 32–41, Winter.
[10] S. Xia, X. Luo, K.W. Chan, M. Zhou, G. Li, Probabilistic transient stability constrained optimal power flow for power systems with multiple correlated uncertain wind generations, IEEE Trans Sustainable Energy 7 (3) (2016) 1133–1144.
[11] P.N. Papadopoulos, J.V. Milanović, Probabilistic framework for transient stability assessment of power systems with high penetration of renewable generation, IEEE Trans Power Syst 32 (4) (2017) 3078–3088.
[12] Y. Yuan, J. Kubokawa, H. Sasaki, A solution of optimal power flow with multicontingency transient stability constraints, IEEE Trans Power Syst 18 (3) (2003) 1094–1102.
[13] D. Gan, R.J. Thomas, R.D. Zimmerman, Stability-constrained optimal power flow, IEEE Trans Power Syst 15 (2) (2000) 535–540.
[14] I.A. Calle, E.D. Castronuovo, P. Ledesma, Maximum loadability of an isolated system considering steady-state and dynamic constraints, Int J Electr Power Energy Syst 53 (2013) 774–781.
[15] P. Ledesma, I.A. Calle, E.D. Castronuovo, F. Arredondo, Multi-contingency TSCOPF based on full-system simulation, IET Gener Transm Distrib 11 (1) (2017) 64–72.
[16] A.A.K. Arani, H. Karami, G.B. Gharehpetian, M.S.A. Hejazi, Review of Flywheel Energy Storage Systems structures and applications in power systems and microgrids, Renew Sustain Energy Rev 69 (2017) 9–18.
[17] H. Chen, T.N. Cong, W. Yang, C. Tan, Y. Li, Y. Ding, Progress in electrical energy storage system: a critical review, Prog Nat Sci 19 (3) (2009) 291–312.
[18] R. Sebastián, R. Peña-Alzola, Control and simulation of a flywheel energy storage for a wind diesel power system, Int J Electr Power Energy Syst 64 (2015) 1049–1056.
[19] H. Silva-Saravia, H. Pulgar-Painemal, J. Mauricio, Flywheel energy storage model, control and location for improving stability: the Chilean case, IEEE Trans Power Syst PP (99) (2016), p. 1–1.
[20] Weckesser T, Jóhannsson H, Østergaard J., Impact of model detail of synchronous machines on real-time transient stability assessment. In: *2013 IREP Symposium Bulk Power System Dynamics and Control – IX Optimization, Security and Control of the Emerging Power Grid*, 2013, pp. 1–9.
[21] P.W. Sauer, M.A. Pai, Power system dynamics and stability, Urbana 51 (1997) 61,801.
[22] B. Bolund, H. Bernhoff, M. Leijon, Flywheel energy and power storage systems, Renew Sustain Energy Rev 11 (2) (2007) 235–258.
[23] M.A. Awadallah, B. Venkatesh, Energy storage in flywheels: an overview, Can J Electr Comput Eng 38 (2) (2015) 183–193, Spring.
[24] 'ABB Group -PowerStore Renewable microgrid stabilization'.
[25] Y. Suzuki, A. Koyanagi, M. Kobayashi, R. Shimada, Novel applications of the flywheel energy storage system, Energy 30 (11–12) (2005) 2128–2143.
[26] J. Beerten, S. Cole, R. Belmans, Generalized steady-state VSC MTDC model for sequential AC/DC power flow algorithms, IEEE Trans Power Syst 27 (2) (2012) 821–829.
[27] Mauricio JM, Maza-Ortega JM, Gómez-Expósito A. 'Considering power losses of switching devices in transient simulations through a simplified circuit model', International Conference on Power System Transients (IPST2009) in Kyoto, Japan June 3–6, 2009, vol. 1, p. 2.
[28] Procedimientos de operación | Red Eléctrica de España'. [Online]. Available: http://www.ree.es/es/actividades/operacion-del-sistema-electrico/procedimientos-de-operacion. [Accessed: 06-Jun-2017].
[29] Siemens Energy Inc, Siemens PTI, PSSE Program Application Guide – 7.2 Load Voltage Characteristics.

[30] P. Kundur, N.J. Balu, M.G. Lauby, Power system stability and control, McGraw-hill, New York, 1994.
[31] I.A. Calle, E.D. Castronuovo, P. Ledesma, Optimal re-dispatch of an isolated system considering transient stability constraints, Int J Electr Power Energy Syst 44 (1) (2013) 728–735.
[32] A. Rabiee, S.M. Mohseni-Bonab, Maximizing hosting capacity of renewable energy sources in distribution networks: a multi-objective and scenario-based approach, Energy 120 (2017) 417–430.
[33] 'Power Flow Cases – Illinois Center for a Smarter Electric Grid (ICSEG)'. [Online]. Available: http://icseg.iti.illinois.edu/power-cases/. [Accessed: 28-Mar-2018].